Progress In Electromagnetics Research, Vol. 116, 297–312, 2011

OPTIMUM DESIGN FOR IMPROVING MODULATING-EFFECT OF COAXIAL MAGNETIC GEAR USING RESPONSE SURFACE METHODOLOGY AND GENETIC ALGORITHM

L. Jian, G. Xu, and J. Song

Shenzhen Institutes of Advanced Technology
Chinese Academy of Sciences & Chinese University of Hong Kong
1068 Xueyuan Avenue, University Town, Shenzhen, P. R. China

H. Xue and D. Zhao

School of Mathematics and Statistics
Huazhong Normal University, 152 Luoyu Avenue, Wuhan, P. R. China

J. Liang

Shenzhen Institutes of Advanced Technology
Chinese Academy of Sciences & Chinese University of Hong Kong
1068 Xueyuan Avenue, University Town, Shenzhen, P. R. China

Abstract—Coaxial magnetic gear (CMG) is a non-contact device for torque transmission and speed variation which exhibits promising potential in several industrial applications, such as electric vehicles, wind power generation and vessel propulsion. CMG works lying on the modulating-effect aroused by the ferromagnetic segments. This paper investigates the optimum design for improving the modulating-effect. Firstly, the operating principle and the modulating-effect is analyzed by using 1-D field model, which demonstrates that the modulating-effect is essential for the torque transmission capacity of CMGs, and the shape of the ferromagnetic segments have impact on the modulating-effect. Secondly, the fitted model of the relationship between the maximum pull-out torque and the shape factors including radial height, outer-edge width-angle and inner-edge width-angle is built up by using surface response methodology. Moreover, FEM is engaged to evaluate its accuracy. Thirdly, the optimum shape of the ferromagnetic segment is obtained by using genetical algorithm.

Received 23 March 2011, Accepted 29 April 2011, Scheduled 6 May 2011
Corresponding author: Linni Jian (ln.jian@siat.ac.cn).

1. INTRODUCTION

As a newly emerging device, coaxial magnetic gears (CMGs) have attracted increasing attention recently. On one hand, they are able to achieve speed variation as well as torque transmission, just like the mechanical gears; On the other hand, they can overcome the disadvantages of their mechanical counterparts, such as, friction loss, audible noise, mechanical vibration and need of regular lubrication and maintenance. Moreover, they are able to offer physical isolation between the input side and the output side, and self-protection when overloaded.

CMG was firstly proposed in [1], in which, a device works lying on the magnetic field modulation was analyzed and simulated. Then, several CMGs with different gear ratios were investigated [2]. Moreover, the thickness of the modulating ring was found to have impact on the maximum pull-out torque of the CMG. In [3], a CMG with the spoke type of permanent magnets (PMs) employed on the inner-rotor was proposed. In order to improve the torque transmission capacity, as well as reduce torque ripples, Halbach PM arrays were adopted on both the inner-rotor and the outer-rotor [4]. In [5], each modulated harmonics was identified, which shows that some of the field harmonics have contribution to the stable torque transmission and the speed variation, while the others just arouse torque ripples. In [6], the surface-inset PMs are used on the outer-rotor, and it also unveils that the width of the ferromagnetic segments on the modulating ring could affect the maximum pull-out torque. In [7] and [8], the magnetic field distribution in the CMG was analytically calculated. Although the nonlinear characteristic of the ferromagnetic materials has not been taken into account, the calculation results were acceptable compared with that obtained by using finite element method (FEM). CMGs also exhibit their potential in several industrial applications, such as wind power generation [9, 10], electric vehicles [11] and ship propulsion [12].

The purpose of this paper is to investigate the optimum design for improving the modulating-effect of the CMG, so as to improve its torque transmission capacity. In Section 2, the modulating effect will be introduced and analyzed by using 1-D field model. In Section 3, response surface methodology [13–15] will be adopted to find out the relationship between the maximum pull-out torque and the shape factors of the ferromagnetic segments. After that, the genetic algorithm will be engaged to determine the optimum design in Section 4. Finally, conclusions will be drawn in Section 5.

2. MODULATING-EFFECT OF COAXIAL MAGNETIC GEAR

As shown in Figure 1, the effective components of the CMG consist of two rotational parts: the outer-rotor and the inner-rotor, and one stationary part: the modulating ring. It can be observed that, PMs are mounted on the inner surface of the outer-rotor, and the outer surface of the inner-rotor, respectively. Ferromagnetic segments are symmetrically deployed on the modulating ring. By defining p_1, p_2 as the pole-pair numbers of the PMs on the outer-rotor and inner-rotor, respectively, and N_s as the number of ferromagnetic segments, when they satisfy:

$$N_s = p_1 + p_2 \tag{1}$$

the operation of the magnetic gear can be given by:

$$\omega_2 = -G_r\omega_1 \tag{2}$$

$$G_r = \frac{p_1}{p_2} \tag{3}$$

where ω_1, ω_2 are the rotational speeds of the outer-rotor and inner-rotor respectively, and G_r is the gear ratio. The minus sign indicates that the two rotors rotate in opposite directions.

The operation of the CMG lies on the modulating-effect of the modulating ring. Assuming that the modulating ring is removed, the PMs on the outer-rotor and the inner-rotor could excite their magnetic fields in the space between the two rotors. It is easy to know that the space pole-pair numbers of the magnetic fields produced by the outer-rotor and the inner-rotor are equal to p_1 and p_2, respectively. Since they do not match with each other, stable torque transmission can not

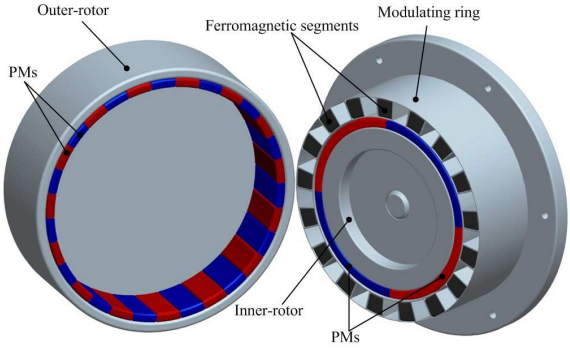

Figure 1. Coaxial magnetic gear.

be achieved, which means when the outer-rotor is dragged to rotate, the inner-rotor will keep still, and vice versa. Once the modulating ring is equipped, it becomes a totally different case. Due to the perfect magnetic conductivity of the ferromagnetic segments, the magnetic field excited by the outer-rotor will be modulated into a field consisting of abundant harmonics, in which, a harmonic component with the pole-pair number equal to p_2 could interact with the magnetic field produced by the inner-rotor. Similarly, the magnetic field excited by the inner-rotor will also be modulated, and there is a harmonic component with the pole-pair number equal to p_1 could interact with the magnetic field produced by the outer-rotor. Actually, there are many other harmonics involved in the torque transmission and speed variation [5].

The modulating-effect can be simply analyzed by using 1-D field model [16]. Figures 2(a) and 2(b) shows the cases when only the PMs on one rotor are taken into account. In 1-D field model, the circumferential component of magnetic field is ignored, and the magnetic flux lines are assumed to go directly up and down in radial direction. Thus, the magnetic flux density excited by the outer-rotor PMs B_{om} and that excited by the inner-rotor PMs B_{im} can be expressed as:

$$B_{om}(\theta) = F_{om}(\theta)P(\theta) \tag{4}$$

$$B_{im}(\theta) = F_{im}(\theta)P(\theta) \tag{5}$$

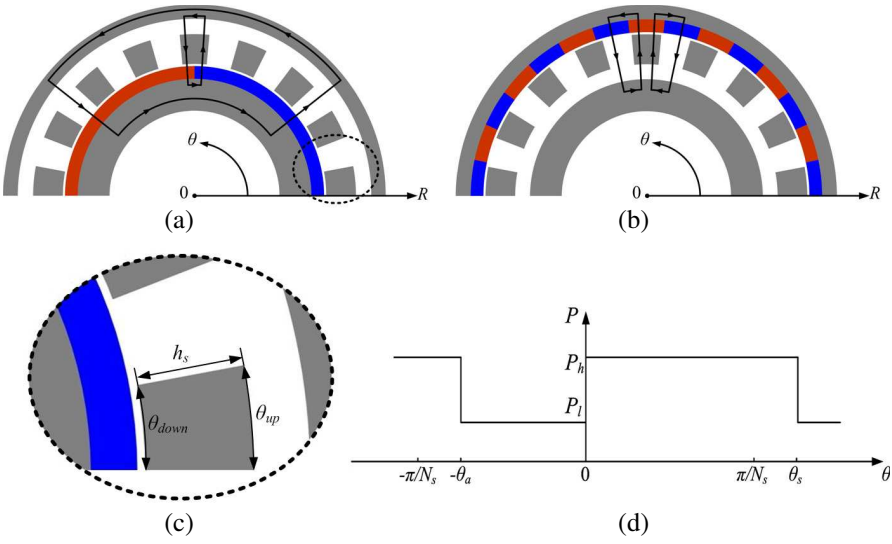

Figure 2. 1-D magnetic field model.

where F_{im}, F_{om} are the magneto motive forces (MMFs) provided by the inner-rotor PMs and the outer-rotor PMs, respectively, and $P(\theta)$ is the magnetic permeance in radial direction. Without considering the high-order harmonics, the MMFs can be written in the form of fundamental components:

$$F_{om}(\theta) = \frac{B_{or}h_{om}\cos p_1(\theta+\omega_1 t+\alpha_0)}{\mu_0} \tag{6}$$

$$F_{im}(\theta) = \frac{B_{ir}h_{im}\cos p_2(\theta+\omega_2 t+\beta_0)}{\mu_0} \tag{7}$$

where B_{or}, h_{om} and α_0 are the remanence, the height in radial direction and the initial phase angle of the outer-rotor PMs, respectively, while, B_{ir}, h_{im} and β_0 are the remanence, the height in radial direction and the initial phase angle of the inner-rotor PMs, respectively.

The ferromagnetic segment is shown in detail in Figure 2(c). θ_{up} and θ_{down} denote the width in circumferential direction of the outer-edge and the inner-edge, respectively, h_s denotes the height in radial direction. Herein, we assume $\theta_{up} = \theta_{down} = \theta_s$, the magnetic permeance can be expressed as:

$$P(\theta) = \frac{1}{\rho_{im}+\rho_{om}+\rho_{ig}+\rho_{og}+\rho_s(\theta)} \tag{8}$$

where $\rho_{im} = h_{im}/\mu_0$, $\rho_{om} = h_{om}/\mu_0$, $\rho_{ig} = h_{ig}/\mu_0$ and $\rho_{og} = h_{og}/\mu_0$ are the magnetic reluctance of the inner-rotor PMs, the outer-rotor PMs, the inner air-gap and the outer air-gap, respectively, $\rho_s(\theta)$ is the magnetic reluctance of the modulating ring, $\rho_s(\theta) = h_s/\mu_0$ when it corresponding to the air-slot, while, $\rho_s(\theta) = 0$ when it corresponding to the ferromagnetic segments, h_{ig} and h_{og} are the height of the inner air-gap and the outer air-gap, respectively.

Consequently, the waveform of the magnetic permeance is shown in Figure 2(d). It can be expanded in form of Fourier series:

$$P(\theta) = P_0 + \sum_{j=1}^{+\infty} P_j \cos jN_s\left(\theta - \frac{\theta_s}{2}\right) \tag{9}$$

$$P_0 = \left(1 - \frac{N_s\theta_s}{2\pi}\right)P_l + \frac{N_s\theta_s}{2\pi}P_h \tag{10}$$

$$P_j = \frac{P_h - P_l}{j\pi}\sqrt{2(1-\cos jN_s\theta_s)} \tag{11}$$

$$P_h = \frac{\mu_0}{h_{im}+h_{om}+h_{ig}+h_{og}} \tag{12}$$

$$P_l = \frac{\mu_0}{h_{im}+h_{om}+h_{ig}+h_{og}+h_s} \tag{13}$$

Substituting (6)–(13) into (4), the fundamental components of the magnetic flux density excited by the outer-rotor PMs can be obtained as:

$$B_{om}^{0} = \frac{P_0 B_{or} h_{om} \cos p_1(\theta + \omega_1 t + \alpha_0)}{\mu_0} \tag{14}$$

Moreover, the first-order harmonic aroused by the modulating-effect can be given by:

$$B_{om}^{1} = \frac{P_1 B_{or} h_{om} \cos p_2 \left(\theta - G_r \omega_1 t + \frac{\alpha_0}{p_2} + \frac{\theta_s}{2p_2}\right)}{\mu_0} \tag{15}$$

Similarly, by substituting (6)–(13) into (5), the fundamental components of the magnetic flux density excited by the inner-rotor PMs can be obtained as:

$$B_{im}^{0} = \frac{P_0 B_{ir} h_{im} \cos p_2(\theta + \omega_2 t + \beta_0)}{\mu_0} \tag{16}$$

In addition, the first-order harmonic aroused by the modulating-effect can be given by:

$$B_{im}^{1} = \frac{P_1 B_{ir} h_{im} \cos p_1 \left(\theta - \frac{1}{G_r}\omega_2 t + \frac{\beta_0}{p_1} + \frac{\theta_s}{2p_1}\right)}{\mu_0} \tag{17}$$

From (14)–(17), It can be found that the components B_{om}^{0} and B_{im}^{1} have the same pole-pair number and the rotational speed. Thus, they can interact with each other to develop stable magnetic torque, In addition, the components B_{im}^{0} and B_{om}^{1} have the same pole-pair number and the rotational speed. Thus, they can also interact with each other to develop stable magnetic torque. The maximum pull-out torques can be given by:

$$T_{\max} = \frac{P_0 P_1 B_{or} B_{ir} h_{om} h_{im} L}{\mu_0^2} \tag{18}$$

where L is the axial length of the CMG.

It can be seen that the term $B_{or}B_{ir}h_{om}h_{im}L$ is corresponding to the magnetic intensity provided by the PMs, while the term P_0P_1 represents the modulating-effect of the modulating ring. With the contribution of both the magnetic intensity and the modulating-effect, the pull-out torque is generated. From (10)–(13), it can be found that the modulating is strongly related to the shape factors of the ferromagnetic segments, such as, the height in radial direction h_s and the width in circumferential direction θ_s. Although the 1-D field model is very convenient for analyzing the modulating-effect and the operating principle of CMG, it is not a satisfactory tool for optimum

design of the ferromagnetic segments since the assumption of ignoring the circumferential component of magnetic field is adopted. Actually, the circumferential component does exist, and has impact on the performance of the CMG.

3. SHAPE FACTORS OF FERROMAGNETIC SEGMENTS AND THEIR IMPACT ON MODULATING-EFFECT

As shown in Figure 2(c), the shape factors of the ferromagnetic segment include the width-angle in circumferential direction of the outer-edge and the inner-edge θ_{up} and θ_{down}, and the height in radial direction h_s. In this section, their impact on the modulating-effect which can be observed from the maximum pull-out torque will be investigated. The other sizes which are kept unchanged are listed in Table 1. The thickness of the inner-rotor PMs h_{im} will change with the h_s, so as to keep the volume of the inner-rotor PMs unchanged.

Response surface methodology (RSM) is a statistical technique for finding the best-fitted relationship between the design variables and the response. Firstly, the true functional relationship can be expressed as:

$$Y = f(X) \tag{19}$$

where Y is the response vector, X is the design variable vector. The form of the true response function f is to be determined. For this case,

Table 1. Unchanged sizes of CMG considered.

Radius of outside surface of outer-rotor	90 mm
Thickness of outer-rotor iron yoke	7 mm
Thickness of outer-rotor PMs	6 mm
Length of outer air-gap	1 mm
Thickness of inner-rotor iron yoke	15 mm

Table 2. Design variables and scaled units.

h_s/x_1	3 mm/-1	16.5 mm/0	30 mm/1
θ_{up}/x_2	3 Deg./-1	10.5 Deg./0	18 Deg./1
θ_{up}/x_2	3 Deg./-1	10.5 Deg./0	18 Deg./1

the second-order model is used to approximate the response function:

$$Y = \beta_0 + \sum_{j=1}^{k} \beta_j x_j + \sum_{i,j=1}^{k} \beta_{ij} x_i x_j + \epsilon \tag{20}$$

where Y denotes the maximum pull-out torque, β is the regression coefficients, ϵ is the random error. The number of the design variables $k = 3$, and x_1, x_2 and x_3 are the centered and scaled design units of h_s, θ_{up} and θ_{down}.

Secondly, the central composite design (CCD) is applied to construct the samples to be investigated. In order to get the comprehensive knowledge of the response function, a wide region of the design variables as shown in Table 2 is investigated. consequently, 15 samples listed in Table 3 are determined.

Thirdly, Finite element method (FEM) is engaged to calculated the maximum pull-out torque of these 15 samples. FEM is a widely acknowledged tool for analyzing and designing electromagnetic devices [17–21]. Figure 3 shows the flux line distributions of the selected simples, and the calculated maximum pull-out torques are given in Table 3.

Fourthly, the least-squares method is used to estimate the

Table 3. Samples to be investigated.

Case No.	h_s (mm)	θ_{up} (Deg.)	θ_{down} (Deg.)	h_{im} (mm)	*Torque* (Nm)
1	30	18	18	8.5445	58.979696
2	30	18	3	8.5445	78.579435
3	30	3	18	8.5445	90.073385
4	30	3	3	8.5445	82.874360
5	3	18	18	5.0075	38.144822
6	3	18	3	5.0075	56.184524
7	3	3	18	5.0075	60.808025
8	3	3	3	5.0075	23.226907
9	16.5	10.5	18	6.2865	119.45689
10	16.5	10.5	3	6.2865	114.90713
11	16.5	18	10.5	6.2865	101.466832
12	16.5	3	10.5	6.2865	99.092563
13	30	10.5	10.5	8.5445	106.96553
14	3	10.5	10.5	5.0075	79.396921
15	16.5	10.5	10.5	6.2865	124.660785

unknown regression coefficients β:

$$\hat{\beta} = (X^T X)^{-1} X^T Y \tag{21}$$

where X^T is the transpose of X. The fitted response Y is given by:

$$\hat{Y} = X\hat{\beta} \tag{22}$$

According to the results listed in Tables 2 and 3, the fitted second-order polynomial function is:

$$\begin{aligned} Y \;=\; & 125.02522 + 1597.112x_1 - 2.27199x_2 + 1.16905x_3 \\ & -31.68510x_1^2 - 24.58663x_2^2 - 7.68432x_3^2 \\ & -5.71038x_1x_2 - 2.399277x_1x_3 - 10.30245x_2x_3 \end{aligned} \tag{23}$$

Finally, the analysis-of-variance (ANOVA) [22] is engaged to examine the fitted model (23) to ensure that it could provide an

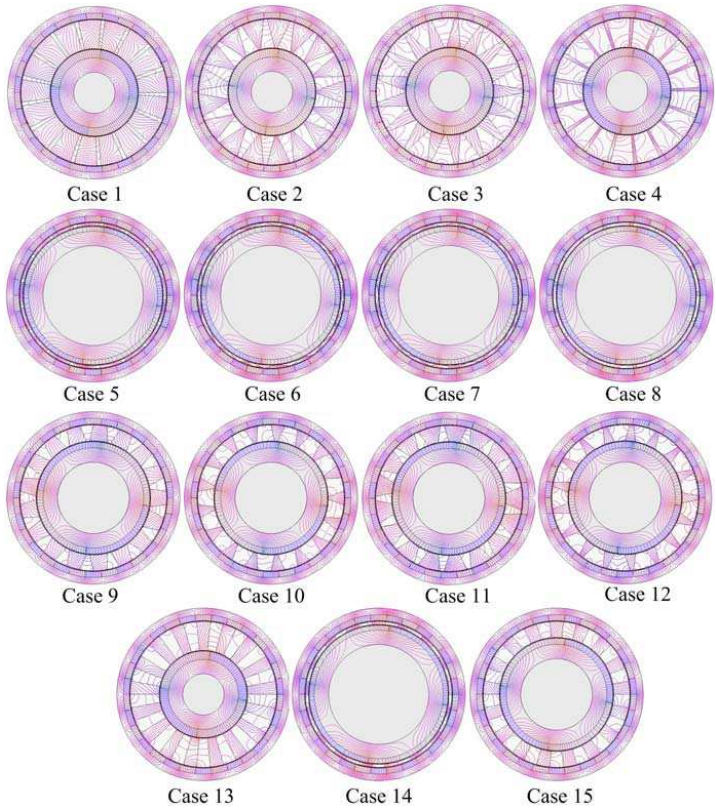

Figure 3. Flux line distribution.

adequate approximation for the true response. Herein, the total number of parameters in the fitted model M is 10, while the number of the simples N equals 15, thus the degree of freedom of the regression and the residual equals 9 and 5, respectively. The total variation is a set of data called the total sum of squares (SST) of deviations of the observed Y_u about their average value $\bar{Y}$:

$$\mathrm{SST} = \sum_{j=1}^{N} \left(Y_u - \bar{Y}^2\right) \tag{24}$$

The SST can be partitioned into two parts, the sum of squares due to regression (SSR) (or sum of squares explained by the fitted model) and the sum of squares unaccounted for by the fitted (or sum squares of error(SSE)). The formula for calculation the SSR is:

$$\mathrm{SSR} = \sum_{j=1}^{N} \left(\hat{Y}_u - \bar{Y}^2\right) \tag{25}$$

where $\hat{Y}_u$ is the predicted value for the u-th case by using the fitted model (23). SSR means the difference between the predicted value and the overall average value observed.

The SSE by the fitted model is:

$$\mathrm{SSE} = \sum_{j=1}^{N} \left(Y_u - \hat{Y}_u^2\right) \tag{26}$$

The coefficient of determination R^2 can be obtained from SST and SSR by:

$$R^2 = \frac{\mathrm{SSR}}{\mathrm{SST}} \tag{27}$$

It is a measure of the proportion of total variation of the values of Y_u about the mean $\bar{Y}$ explained by the fitted model. A related statistic, named the adjusted coefficient of determination R_A^2 is given by:

$$R_A^2 = 1 - \frac{\mathrm{SSE}/(N-M)}{\mathrm{SST}/(N-1)} \tag{28}$$

It is a measure of the proportion of the estimate of the error variance provided by the residual mean square of the error variance estimate using the total mean square. Table 4 shows the results of ANOVA. It can be seen that the coefficient of determination R^2 is 0.9883, while the adjusted coefficient of determination R_A^2 equals 0.9673. This means that the second-order polynomials have a good accuracy for this range of design variables.

The comparison between the 'true' value calculated by using FEM and the fitted value calculated by using the fitted model (23) is illustrated in Figures 4 and 5. In Figure 4, θ_{up} is chosen to be equal to θ_{down}, and denoted by θ, and the variation of the maximum pull-out torque with h_s and θ is plotted. In Figure 5, h_s is chosen to be 15 mm, and the variation of the maximum pull-out torque with θ_{up} and θ_{down} is plotted. Obviously, the shape of the fitted response surface is very close to that of the 'true' response surface.

4. DESIGN OPTIMIZATION

Since the fitted model (23) could approximate the impact of the shape factors of ferromagnetic segments on the torque transmission capacity with good accuracy, in this section, the optimum solution that results in the maximum pull-out torque will be analyzed. The optimization

Table 4. Analysis of variance.

Source	Regression	Residual	Total
Degree of Freedom	9	5	14
Sum of Squares	12642	149.33340	12792
Mean Square	1404.71215	29.86668	-
F-Statistic	47.03	-	-
Coefficient of Determination R^2	0.9883	-	-
Adjusted Coefficient of Determination R_A^2	0.9673	-	-

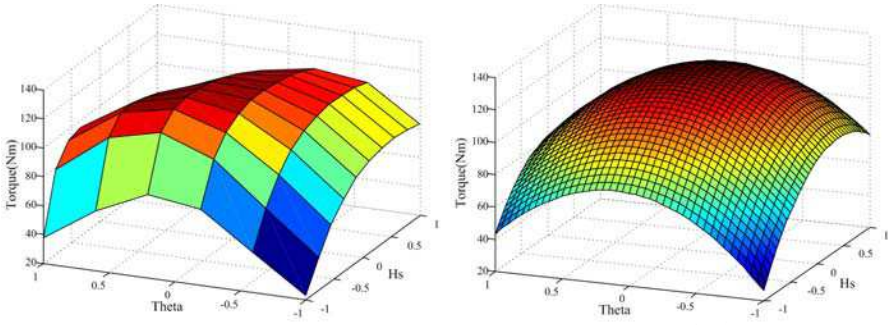

Figure 4. Comparison of response surfaces over $\{\theta_{up} = \theta_{down} \in [3, 18],\ h_s \in [3, 30]\}$. (a) True value. (b) Fitted value.

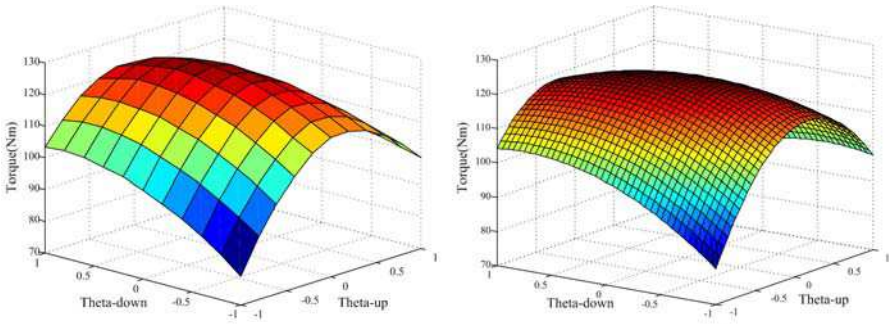

(a) (b)

Figure 5. Comparison of response surfaces over $\{\theta_{up} \in [3, 18],\ \theta_{down} \in [3, 18],\ h_s = 15\}$. (a) True value. (b) Fitted value.

problem is given by:

$$\begin{aligned} &\min -Y = -f(X) \\ \text{s.t.} \quad &\{X = [x_1, x_2, x_3]^T; x_1 \in [-1, 1]; x_2 \in [-1, 1]; x_3 \in [-1, 1]\} \end{aligned} \tag{29}$$

where the function $Y = f(X)$ is given in (23).

Genetic algorithm [23–25] is engaged to solve this problem. Firstly, the first generation of chromosomes is randomly generated. The number of chromosomes is also named as population size. Usually, the population size can range from 50–1000 according to the accuracy required and the complexity of the problem. Herein, the population size is chosen as 50. Once the initial population is generated, the performance of the objective function is evaluated. The chromosome which could result in the minimum value of the objective function will be reproduced in the next generation. While, the others will be operated by either the crossover operation or mutation operation, so as to produce the new chromosomes of the next generation. Inspired by the role of natural selection in evolution, the genetic algorithm will repeat the aforementioned process of evaluation, selection and generation to keep the "most fit" chromosome survive, and the "least fit" chromosome eliminated. Once the average change in the fitness value is less than the predetermined upper bound, the optimization will be terminated, and the optimum solution is obtained.

Figure 6(a) shows the history of genetic algorithm optimization at each generation. It can be seen that after 30th iterations, the fitted maximum pull-out torque is kept unchanged, which is equal to 127.2087 Nm. The optimal solution is $x_1 = 0.2559$, $x_2 = -0.0908$ and $x_3 = 0.0700$. After transformation, it yields that $h_s = 19.95465$ mm, $\theta_{up} = 9.819$ Deg. and $\theta_{down} = 11.025$ Deg.. Finally, the FEM

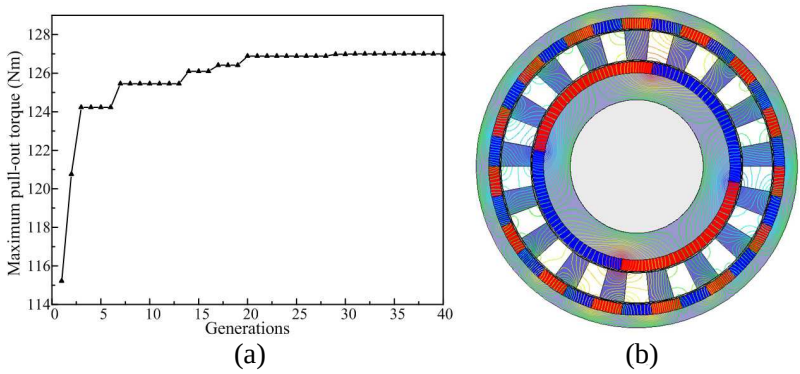

Figure 6. Optimization using genetic algorithm. (a) Maximum pullout torque at each generation. (b) Flux line distribution in optimal case.

is used to evaluate the optimum case. Its flux line distribution is plotted in Figure 6(b), and the calculated maximum pull-out torque is 126.21623 Nm, which agrees well with the value given by the fitted model.

5. CONCLUSIONS

In this paper, the optimum design for improving the modulating-effect of coaxial magnetic gear (CMG) is investigated. Firstly, the operating principle and the modulating-effect of CMG is analyzed by using 1-D field model, which demonstrates that the modulating-effect is essential for the torque transmission capacity of CMGs, and the shape of the ferromagnetic segments have impact on the modulating-effect. Secondly, the fitted model of the relationship between the maximum pull-out torque and the shape factors including radial height, outer-edge width-angle and the inner-edge width-angle is built up by using surface response methodology. Moreover, FEM is engaged to evaluate its accuracy. Thirdly, the optimum shape of the ferromagnetic segment is obtained by using genetical algorithm.

REFERENCES

1. Atallah, K. and D. Howe, "A novel high-performance magnetic gear," *IEEE Trans. Magn.*, Vol. 37, No. 4, 2844–2846, 2001.
2. Atallah, K., S. Calverley, and D. Howe, "Design, analysis and

realization of a high-performance magnetic gear," *IEE Proc. Electric Power Appl.*, Vol. 151, No. 2, 135–143, 2004.

3. Rasmussen, P., T. Andersen, F. Jorgensen, and O. Nielsen, "Development of a high-performance magnetic gear," *IEEE Trans. Ind. Appl.*, Vol. 41, No. 3, 764–770, 2005.
4. Jian, L., K. T. Chau, Y. Gong, J. Jiang, C. Yu, and W. Li, "Comparison of coaxial magnetic gears with different topologies," *IEEE Trans. Magn.*, Vol. 45, No. 10, 4526–4529, 2009.
5. Jian, L. and K. T. Chau, "A coaxial magnetic gear with halbach permanent-magnet arrays," *IEEE Trans. Energy Conversion*, Vol. 25, No. 2, 319–328, 2010.
6. Liu, X., K. T. Chau, J. Jiang, and C. Yu, "Design and analysis of interior-magnet outer-rotor concentric magnetic gears," *Journal of Applied Physics*, Vol. 105, No. 7, 1–3, 2009.
7. Jian, L. and K.-T. Chau, "Analytical calculation of magnetic field distribution in coaxial magnetic gears," *Progress In Eletromagnetics Research*, Vol. 92, 1–16, 2009.
8. Lubin, T., S. Mezani, and A. Rezzoug, "Analytical computation of the magnetic field distribution in a magnetic gear," *IEEE Trans. Magn.*, Vol. 46, No. 7, 2611–2621, 2010.
9. Jian, L., K. T. Chau, and J. Jiang, "A magnetic-geared outer-rotor permanent-magnet brushless machine for wind power generation," *IEEE Trans. Ind. Appl.*, Vol. 45, No. 3, 954–962, 2009.
10. Jian, L., G. Xu, Y. Gong, J. Song, J. Liang, and M. Chang, "Electromagnetic design and analysis of a novel magnetic-gear-integrated wind power generator using time-stepping finite element method," *Progress In Eletromagnetics Research*, Vol. 113, 351–367, 2011.
11. Jian, L. and K.-T. Chau, "Design and analysis of a magnetic-geared electronic-continuously variable transmission system using finite element method," *Progress In Eletromagnetics Research*, Vol. 107, 47–61, 2010.
12. Frank, N. and H. Toliyat, "Gearing ratios of a magnetic gear for marine applications," *IEEE Electric Ship Technologies Symposium, ESTS 2009*, 477–481, 2009.
13. Hong, D., B. Woo, D. Koo, and D. Kang, "Optimum design of transverse flux linear motor for weight reduction and improvement thrust force using response surface methodology," *IEEE Trans. Magn.*, Vol. 44, No. 11, 4317–4320, 2008.
14. Choi, Y., H. Kim, and J. Lee, "Optimum design criteria for maximum torque density and minimum torque ripple of

SynRM according to the rated wattage using response surface methodology," *IEEE Trans. Magn.*, Vol. 44, No. 11, 4135–4138, 2008.

15. Hasanien, H., A. Abd-Rabou, and S. Sakr, "Design optimization of transverse flux linear motor for weight reduction and performance improvement using response surface methodology and genetic algorithms," *IEEE Trans. Energy Conversion*, Vol. 25, No. 3, 598–605, 2010.
16. Jian, L., K. T. Chau, W. Li, and J. Li, "A novel coaxial magnetic gear using bulk HTS for industrial applications," *IEEE Trans. Appl. Superconduc.*, Vol. 20, No. 3, 981–984, 2010.
17. Faiz, J. and B. M. Ebrahimi, "Mixed fault diagnosis in three-phase squirrel-cage induction motor using analysis of air-gap magnetic field," *Progress In Eletromagnetics Research*, Vol. 64, 239–255, 2006.
18. Vaseghi, B., N. Takorabet, and F. Meibody-Tabar, "Transient finite element analysis of induction machines with stator winding turn fault," *Progress In Eletromagnetics Research*, Vol. 95, 1–18, 2009.
19. Faiz, J., B. M. Ebrahimi, and M. B. B. Sharifian, "Time stepping finite element analysis of broken bars fault in a three-phase squirrel-cage induction motor," *Progress In Eletromagnetics Research*, Vol. 68, 53–70, 2007.
20. Touati, S., R. Ibtiouen, O. Touhami, and A. Djerdir, "Experimental investigation and optimization of permanent magnet motor based on coupling boundary element method with permeances network," *Progress In Eletromagnetics Research*, Vol. 111, 71–90, 2011.
21. Lecointe, J.-P., B. Cassoret, and J. F. Brudny, "Distinction of toothing and saturation effects on magnetic noise of induction motors," *Progress In Eletromagnetics Research*, Vol. 112, 125–137, 2011.
22. Li, J., Z. Liu, M. Jabbar, and X. Gao, "Design optimization for cogging torque minimization using response surface methodology," *IEEE Trans. Magn.*, Vol. 40, No. 2, 1176–1179, 2004.
23. Siakavara, K., "Novel fractal antenna arrays for satellite networks: Circular ring sierpinski carpet arrays optimized by genetic algorithms," *Progress In Eletromagnetics Research*, Vol. 103, 115–138, 2010.
24. Reza, A. W., M. S. Sarker, and K. Dimyati, "A novel integrated mathematical approach of ray-tracing and genetic algorithm for optimizing indoor wireless coverage," *Progress In Eletromagnetics*

Research, Vol. 110, 147–162, 2010.

25. Agastra, E., G. Bellaveglia, L. Lucci, R. Nesti, G. Pelosi, G. Ruggerini, and S. Selleri, "Genetic algorithm optimization of high-efficiency wide-band multimodal square horns for discrete lenses," *Progress In Eletromagnetics Research*, Vol. 83, 335–352, 2008.